



Cite this: *Nanoscale*, 2022, **14**, 18217

Potential use of bioactive nanofibrous dural substitutes with controlled release of IGF-1 for neuroprotection after traumatic brain injury†

Yue Wang,^{a,b} Qingxia Guo,^b Wei Wang,^c Yuanfei Wang,^{*d} Kuanjun Fang,^c Qi Wan,^b Huanting Li^{*a} and Tong Wu^{ib} ^{*b,c}

For patients suffering from traumatic brain injury (TBI), the closure of dural defects after decompressive craniectomy is the prerequisite to restoring normal physiological functions. It is also an urgent challenge to provide a neuroprotection effect against the primary and secondary nerve damage during long-term recovery. To solve these issues, we herein develop a class of bioactive, nanofibrous dural substitutes that can long-term release insulin-like growth factor 1 (IGF-1) for improving the survival and neurite outgrowth of neural cells after TBI. Such dural substitutes were polycaprolactone (PCL) nanofibers encapsulated with hyaluronic acid methacryloyl (HAMA)/IGF-1 by blend or coaxial electrospinning techniques, achieving bioactive PCL/HAMA/IGF nanofibrous dural substitutes with different release profiles of IGF-1. The nanofibrous dural substitutes exhibited good mechanical properties and hydrophobicity, which prevent cerebrospinal fluid leakage, maintain normal intracranial pressure, and avoid external impact on the brain. We also found that the viability and neurite outgrowth of SH-SY5Y cells and primary neurons were significantly enhanced after neurite transection or oxygen and glucose deprivation treatment. Taken together, such PCL/HAMA/IGF nanofibrous dural substitutes hold promising potential to provide neuroprotection effects after primary and secondary nerve damage in TBI, which would bring significant benefits to the field of neurosurgery involving the use of artificial dura mater.

Received 31st October 2022,
Accepted 7th November 2022

DOI: 10.1039/d2nr06081g

rsc.li/nanoscale

1. Introduction

Traumatic brain injury (TBI) is a temporary or permanent impairment of brain function caused by vigorous acceleration or external forces to the head.^{1,2} There are more than 50 million new TBI cases every year, and the mortality rate exceeds 30% in severe TBI patients.² Decompressive craniectomy is a typical surgical procedure for severe TBI treatment by

removing the skull and dura. However, dural defects usually lead to intracranial infections, cerebrospinal fluid (CSF) leakage, epilepsy, *etc.*³ To solve these complications caused by dural defects, dural substitutes are pivotal to repair and close the dura mater. Currently, there are 5 main types of biomaterials used for dural repairment: homogeneous materials, decellularized materials, natural materials, synthetic materials, and composite materials.⁴ Homogeneous materials are non-toxic and non-immunogenic, but their use is considerably limited due to insufficient tissue sources, additional incisions, viral infections, and ethical reasons.^{4,5} Decellularized materials (*e.g.*, small intestinal submucosa⁶) and natural materials (*e.g.*, collagen,^{7,8} silk fibroin⁹) have excellent biocompatibility but with poor mechanical properties and complicated purification processes. Synthetic materials such as polycaprolactone (PCL)¹⁰ have good mechanical and degradation properties, but their poor cell affinity and adhesion hamper cell growth and proliferation.¹¹

In order to overcome these limitations, composite materials constructed by electrospinning technology have been developed.¹² As the components of composite materials, PCL, hyaluronic acid (HA), and hyaluronic acid methacryloyl (HAMA) have been widely studied in biomedical and tissue engineering applications. PCL is a versatile synthetic polymer with

^aDepartment of Neurosurgery, Affiliated Hospital of Qingdao University, Qingdao 266071, China. E-mail: twu@qdu.edu.cn

^bInstitute of Neuroregeneration and Neurorehabilitation, Qingdao Medical College, Qingdao University, Qingdao 266071, China

^cShandong Key Laboratory of Medical and Health Textile Materials, Collaborative Innovation Center for Eco-textiles of Shandong Province and the Ministry of Education, Qingdao 266071, China

^dDepartment of Central Laboratory, Qingdao Stomatological Hospital Affiliated to Qingdao University, Qingdao 266001, China

†Electronic supplementary information (ESI) available: The degradational mechanical properties (Table S1) and the contact angle and diameter distribution chart (Fig. S1) and degradational SEM images (Fig. S2) of the artificial dural scaffolds; cell viability before and 24 h after axonal transection (Fig. S3); the fluorescence diagram (Fig. S4) and statistic results (Fig. S5) of neurite outgrowth staining before and 24 h after axon transection, and the neurite outgrowth staining of the TCP group (Fig. S6); immunofluorescence staining of primary neurons (Fig. S7). See DOI: <https://doi.org/10.1039/d2nr06081g>

high biocompatibility, biodegradability, and mechanical properties.^{13–15} Simultaneously, PCL produces little acidic products during the degradation and may not generate local inflammatory responses.¹⁶ It has been used as electrospun scaffolds in various biomedical fields and tissue engineering, such as peripheral nerve engineering,¹⁷ cartilage tissue engineering,¹⁸ bone tissue engineering,^{14,15} periodontal tissue engineering,¹⁹ and skin tissue engineering.^{13,20} However, PCL nanofibrous scaffolds are hydrophobic, so pure PCL nanofibers exhibit poor cell adhesion and proliferation properties.²¹ As a natural hydrogel, HA is a significant component of the extracellular matrix in the central nervous system, with good biocompatibility, biodegradability and low immunogenic properties.^{22–27} HA was chemically modified with methacrylate groups to form a HAMA hydrogel, thereby improving its poor cell adhesiveness and mechanical properties.^{26–31} Di Chuan *et al.* developed a stereo complexed composite nanofiber membrane based on poly(lactic acid) by electrospinning, and this dura mater substitute showed the same ultimate tensile strength and elongation at break as human dura mater.³² Rui Shi *et al.* prepared an electrospun PCL–gelatin hybrid membrane with high tensile strength, biocompatibility, and adjustable biodegradation behaviour.¹⁶ However, the above nanofibrous scaffolds or membranes have a little neuroprotective effect on damaged brain tissue.

Insulin-like growth factor 1 (IGF-1) is considered a bioactive and neuroprotective factor that can inhibit neuronal apoptosis and promote neuronal survival and neurite regeneration.^{33–37} Therefore, based on the above analysis, PCL, HAMA, and IGF-1 were used to construct dural substitutes capable of promoting neuronal survival and neurite regeneration and regulate the rapid and long-term release of IGF-1 by two different electrospinning methods (blend and coaxial) to reduce primary and secondary damage caused by postoperative brain injury, thus improving the prognosis of TBI.^{38,39} The results showed that the bioactive dural substitutes have excellent biocompatibility, biodegradability, and mechanical properties. In addition,

after co-culturing with damaged SH-SY5Y cells and primary neurons, the dural substitutes exhibit excellent neuroprotective properties. Therefore, they can provide a promising option for the repair of dura mater after TBI.

2. Experimental section

2.1 Materials

PCL was purchased from Sigma-Aldrich. HAMA and lithium phenyl-2,4,6-trimethylbenzoylphosphinate (LAP) were purchased from EFL (Engineering For Life). IGF-1 antibody was purchased from Beijing Biosynthesis Biotechnology Co., Ltd (China). Hexafluoroisopropanol (HFIP) was purchased from Shanghai Macklin Tech. Co., Ltd (China). Lactate dehydrogenase (LDH) activity assay kit was purchased from Nanjing Jiancheng Bioengineering Tech. Co., Ltd (China).

2.2 Preparation of bioactive nanofibrous dural substitutes (BNDSSs)

BNDSSs were prepared by electrospinning. PCL was added to HFIP with a final mass ratio of 12% (w/v) and stirred thoroughly using a magnetic stirrer until PCL was completely dissolved. HAMA-150k and HAMA-400k were added to LAP at a final mass ratio of 2% and 1% (w/v), respectively, and then heated to 45 °C until HAMA was completely dissolved. As for the blend groups, a mixture of PCL solution and HAMA solution was stirred thoroughly to finally obtain a mixture of PCL/HAMA-150k-B and PCL/HAMA-400k-B. For PCL/HAMA-150k-B/IGF and PCL/HAMA-400k-B/IGF, an additional 50 µg of IGF-1 was added to the mixture. As for the coaxial groups, the PCL solution was the shell solution, the HAMA-150k solution was the core solution (PCL/HAMA-150k-C). For PCL/HAMA-150k-C/IGF, an additional 50 µg of IGF-1 was added to the core solution. When electrospinning was performed, the flow rate of the blend groups was set to 1.0 mL h⁻¹. As for the coaxial groups, the shell and core flow rates were 1.5 mL h⁻¹ and 0.2 mL h⁻¹, respectively. The voltage was set to 15 kV (ET-3556H) at a distance of 15 cm, and the electrospinning time was 3 h. The bioactive artificial dural scaffolds were irradiated under UV light for 20 s and dried in a fume hood to remove the residual solvent.

2.3 Characterization

The fiber morphologies of different BNDSSs were observed using a scanning electron microscope (VEGA 3 SBH, TESCAN). One hundred fibers on SEM photographs were randomly selected, and the average diameter of the fibers was measured using ImageJ software. PCL/HAMA-150k-C/IGF was prepared according to the above procedure, with FITC-BSA (green fluorescence) in the core layer and rhodamine-b (RB, red fluorescence) in the shell layer. To observe the core–shell structure, we used an upright fluorescent microscope (Nikon A1MP, Japan). The tensile mechanical properties of BNDSSs were investigated using a microcomputer control electronic universal testing machine (WDW-5G, Jinan Hengsi Shengda Co., Ltd



Tong Wu

Tong Wu received her Ph.D. in Biomaterials Science from Donghua University in 2018 under the guidance of Prof. Xiumei Mo. She worked in Prof. Younan Xia's group at Georgia Institute of Technology in 2016 as a jointly-supervised Ph.D. candidate and then as a postdoctoral fellow until the end of 2019. She is now working as a professor at Qingdao University. Her research interests include the development of novel nano-

materials for biomedical, environmental and energy-related applications.

China). Briefly, the BNDSSs were first to cut into rectangles with a size of 0.5×2.5 cm, and the thickness of each sample was measured using a screw micrometer. The BNDSSs were tested at a 50 mm min^{-1} tensile speed until fracture occurs. At least three specimens were tested for each BNDSS. Finally, the water contact angles of BNDSSs were measured using a contact angle analyzer (WCA, SA100) at room temperature to detect the hydrophilicity and hydrophobicity of the dural substitutes.

2.4 *In vitro* release study

A 45-day release study was conducted to observe the release rate of the payloads from BNDSSs. The prepared BNDSSs loading 1 mg mL^{-1} RB instead of IGF-1 (50 mg, $n = 3$) were immersed in PBS. The centrifuge tubes were placed in a thermostatic shaker at 37°C and 120 rpm. The PBS was removed on days 1, 3, 5, 7, 10, 15, 20, 30, and 45, and the OD at 560 nm was measured. Before conducting the release study, we first calculated the RB loading rate by the ratio of the amount of RB in the BNDSSs to the initial amount of RB in the solution.⁴⁰ First, BNDSSs were completely dissolved in 10 mL of dichloromethane (DCM), then 10 mL of ddH₂O was added, and a layered solution was obtained after 30 min of vigorous stirring. The OD value at 560 nm of the aqueous phase was measured, and the encapsulation efficiency (EE) and loading capacity (LC) of the RB-loaded BNDSSs were calculated using the following equations.⁴¹

$$\text{EE (\%)} = \frac{\text{Detected amount of drug (mg) in the scaffolds}}{\text{Theoretical amount of drug (mg) in the scaffolds}} \times 100\%$$

$$\text{LC (\%)} = \frac{\text{Detected amount of drug (mg) in the scaffolds}}{\text{Theoretical scaffolds weight (mg)}} \times 100\%$$

2.5 *In vitro* biodegradation study

A degradation study of BNDSSs was performed by examining the weight changes, pH, tensile properties, and microstructures of the BNDSSs after immersion in PBS (pH = 7.35). The prepared scaffolds (50 mg, three samples of each group) were immersed in PBS and later placed in a constant temperature shaker at 37°C and 120 rpm. The BNDSSs were removed and dried on days 10, 20, 30, 60, 90, 120, 150, 180, 270 and 360. The pH of PBS, the weight, tensile strength and the SEM microstructure of BNDSSs were measured.

2.6 Cell cultivation

SH-SY5Y cells were cultured in high glucose Dulbecco's modified Eagle's medium (DMEM, Solarbio, China) supplemented with 10% certified fetal bovine serum (FBS, BI, Israel) and sub-cultured once every two days using trypsin-EDTA solution (MAO232, Meilunbio). Primary neurons were extracted from the cerebral cortex of Sprague Dawley (SD) rats at embryonic day 18 (E18) according to a modified standard protocol.⁴² Briefly, the fresh cortex was digested with 0.05% trypsin and

then inactivated with DMEM containing 10% FBS. Neurons were inoculated at 10^5 cells per well in 24-well culture plates covered with 14 mm PDL-coated coverslips (BS-14-RC, Biosharp). Before the treatment, neurons were continuously incubated in Neurobasal medium (21103-049, Gibco) supplemented with 2% B27 (17504044, Gibco) and 0.5 mmol L^{-1} glutamine (35050061, Gibco). All animal procedures were performed in accordance with the Guidelines for Care and Use of Laboratory Animals of Qingdao University and approved by the Animal Ethics Committee of Affiliated Hospital of Qingdao University.

Neurons were identified by the immunofluorescence staining method. First, the neurons were fixed with 4% paraformaldehyde solution (PFA, Biosharp), followed by blocking with 3% bovine serum albumin (BSA, 9048-46-8, Solarbio) and 0.1% Triton X-100 (9002-93-1, Solarbio) containing PBS for 1 h at room temperature. Subsequently, antibodies to general neuronal markers (Anti-MAP₂, ab5392, 1:2000, Abcam) and neuronal nuclei protein (Anti-NeuN, ab177487, 1:1000, Abcam) were incubated overnight at 4°C . The coverslips were washed with PBS containing 0.1% Tween 20 (9005-64-5, Solarbio) and incubated with the secondary antibody mixture (goat anti-rabbit immunoglobulin G (IgG) (H ± L) FITC, ab6717, 1:500, Abcam and goat anti-chicken immunoglobulin Y (IgY) (H ± L), ab150171, 1:500, Abcam) at 37°C for 1 h. Fluorescence microscopy (Nikon A1MP, Japan) was used for photography. All experiments were approved by and conducted by the Animal Ethics Committee of the Affiliated Hospital and Qingdao Medical College of Qingdao University.

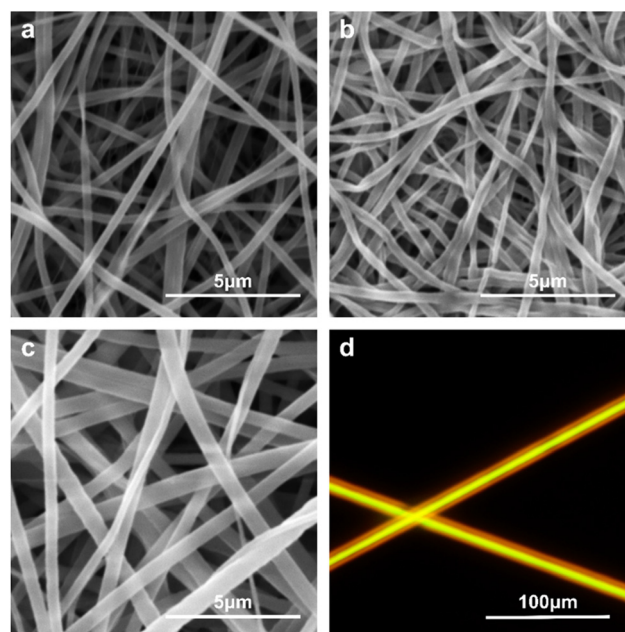


Fig. 1 Characterization. SEM images of (a) PCL/HAMA-150k-B/IGF, (b) PCL/HAMA-400k-B/IGF, and (c) PCL/HAMA-150k-C/IGF BNDSSs. (d) Fluorescence micrograph showing the core-shell structure of one individual PCL/HAMA-150k-C/IGF nanofiber. FITC-BSA was loaded in the core layer (green), and RB was loaded in the shell layer (red).

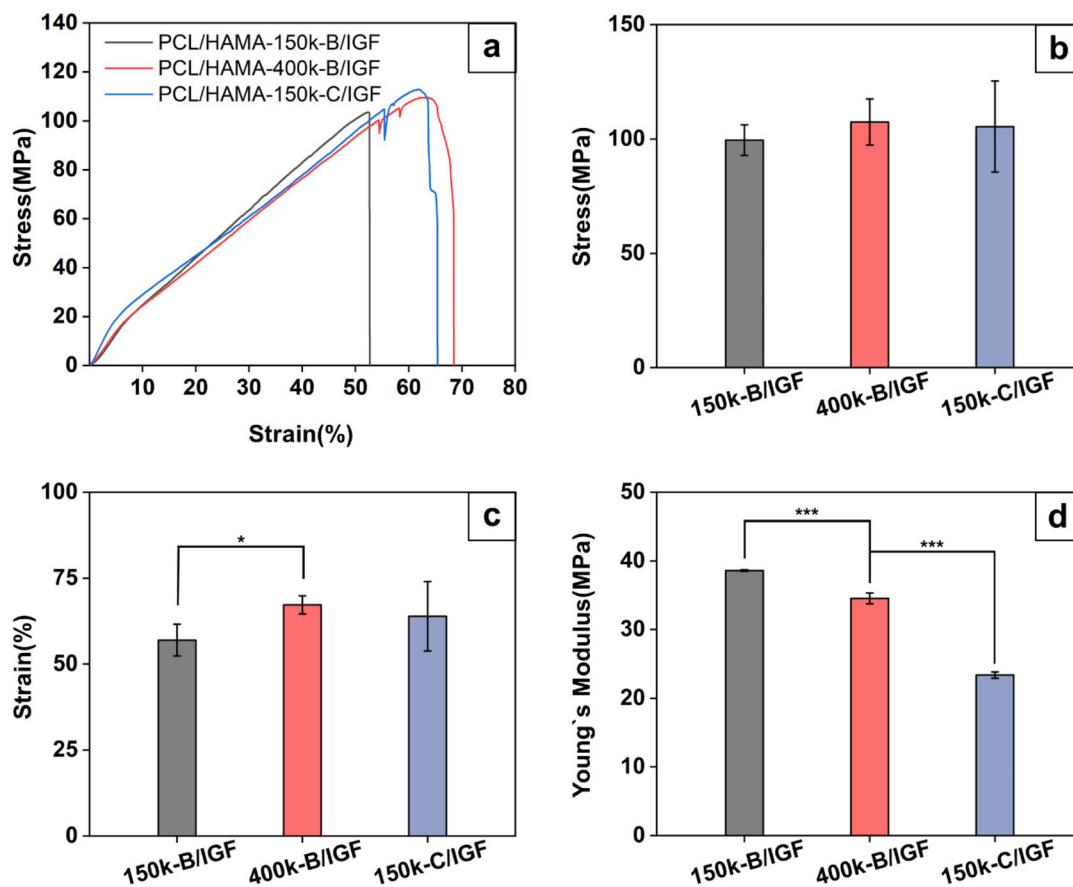


Fig. 2 Mechanical properties. (a) Tensile stress–strain curves. (b) Ultimate strength. (c) Elongation at break. (d) Young's modulus. * $P < 0.05$ and *** $P < 0.001$ indicate the significant differences between the groups.

2.7 Neurite transection experiments

SH-SY5Y cells were cultured at a density of 500 per well in 24-well plates for 1 day, and then cellular neurons were transected 10 times in each well under a microscope (CKX53, OLYMPUS, Japan) with a sterilized fine needle.⁴³ Tissue culture polystyrene (TCP) was used as a control group. In the experimental groups, a co-culture system was established to examine the neuroprotective effects of BNDs on the cells. The BNDs were placed in Transwell chambers (LABSELECT, 6.5 mm diameter for a 24 well plate, 8 μ m polyester membrane) and 24-well plates. Before cell seeding, BNDs were sterilized with 75% ethanol for 12 h and then irradiated with UV light for 30 min. Cell viability was measured using cell counting kit-8 (CCK-8, NCM). After 1 a03/12/22 at 10:57:52 "rscuser5"nd 3 days of incubation, 10% CCK-8 solution (40 μ L in 400 μ L DMEM) was added to each well and incubated for 1.5 hours at 37 $^{\circ}$ C. The optical density values at 450 nm were then measured using a microplate reader (Spectramax ABS, Molecular Devices). Finally, cell viability was determined according to the following equation.

$$\text{Cell viability (\%)} = \frac{\text{Absorbance at 450 nm}}{\text{TCP absorbance at 450 nm}} \times 100\%$$

According to the manufacturer's instructions, the neurite outgrowth was stained with Molecular Probes® Neurite

Outgrowth Staining Kit (ThermoFisher Scientific, A15001). The results were observed using an inverted fluorescence microscope (IX53, OLYMPUS, Japan). One hundred cells from each

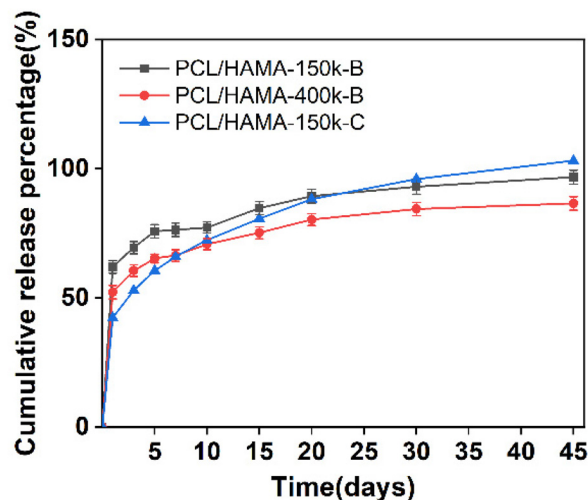


Fig. 3 Release behaviors. Cumulative release curves of payloads from the PCL/HAMA-150k-B, PCL/HAMA-400k-B, and PCL/HAMA-150k-C nanofibrous scaffolds, respectively.

group were randomly selected for statistical analysis. Image J was used to measure each cell's neurite length and number. The neurite length was the average length of all neurites in each cell. The neurite number was the average number in each cell. As for the primary neurons, the neurite transection and co-culturing were performed as described above. After incubation for 1, 3, and 5 days, cell viability assays were performed as described previously. Additionally, after incubation for 3 days, immunofluorescence staining was performed as previously described. We used anti-synaptophysin (SYP, ab32127, 1:1000, Abcam) and anti-MAP₂ (ab5392, 1:2000, Abcam) as the primary antibodies. The neurite length and neurite number were statistically analyzed as previously described.

2.8 Oxygen and glucose deprivation (OGD) experiments

SH-SY5Y cells were seeded in 24-well plates at a density of 5000 cells per well for 12 hours. The cells were refreshed with a deoxygenated glucose-free extracellular solution (in mM: 116 NaCl, 5.4 KCl, 0.8 MgSO₄, 1.0 NaH₂PO₄, 1.8 CaCl₂, and 26 NaHCO₃)⁴⁴ and then immediately placed in a sealed crisper box with an anaerobic bag (C-1, MGC) and incubated at 37 °C with 5% CO₂. After 3 hours, the medium was replaced with high glucose DMEM containing 10% FBS. The plates were returned to 37 °C and 5% CO₂ conditions for reperfusion. Meanwhile, a co-cultured system was established as described previously. Cell viability assays and neurite outgrowth staining

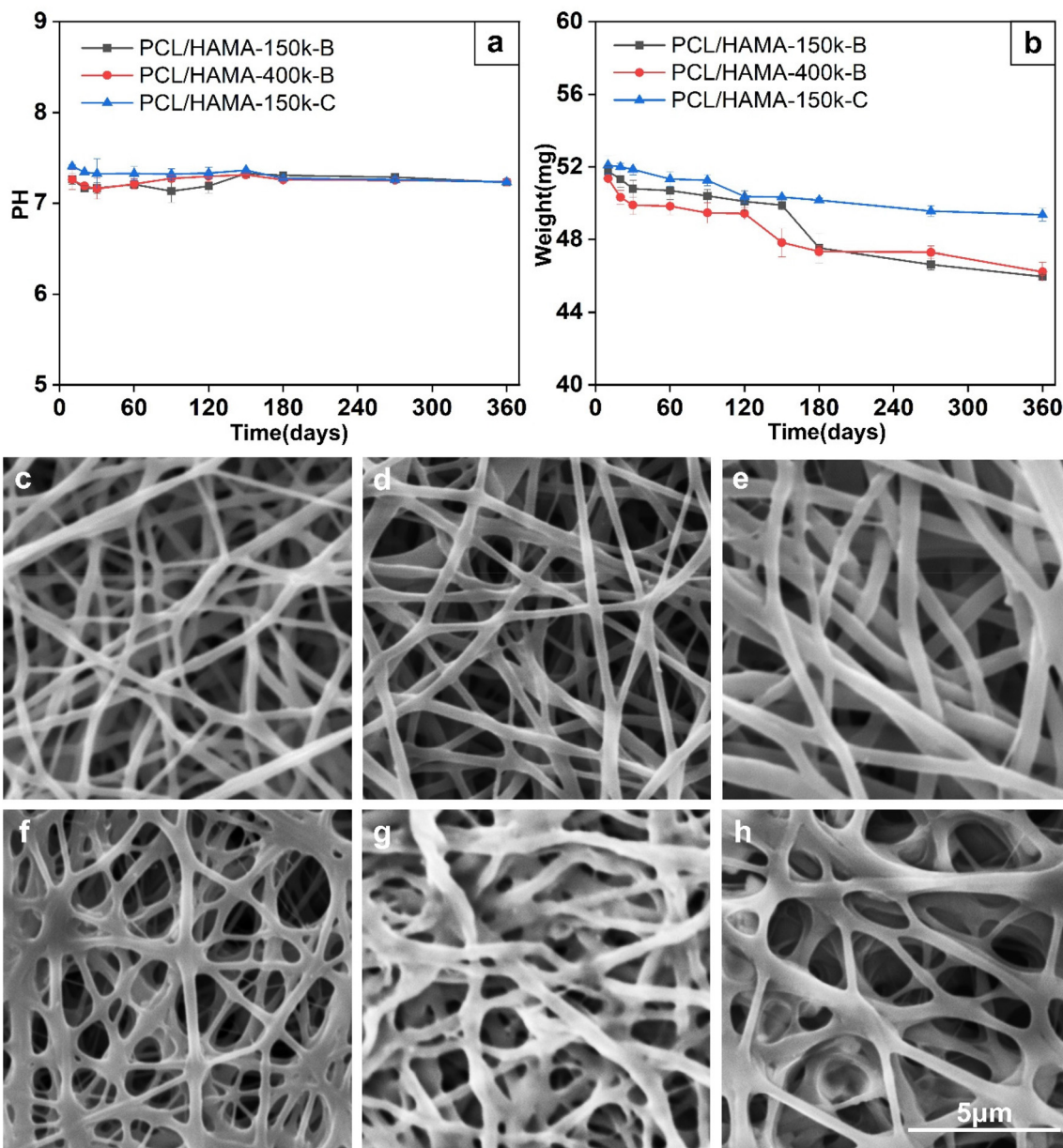


Fig. 4 Degradation behavior. (a) pH curves. (b) Weight loss curves. SEM images showing the fiber morphologies post-degradation at (c–e) 30 days and (f–h) 180 days: (c and f) PCL/HAMA-150k-B; (d and g) PCL/HAMA-400k-B; and (e and h) PCL/HAMA-150k-C.

were performed as described above. The OGD treatment and co-culturing were performed for the primary neurons as described before. After incubation for 1, 3, and 5 days, cell viability assays were performed as described previously. In addition, immunofluorescence staining and statistical analysis of neurons were performed at 3 days post-culture. The LDH activity assay was performed according to the instructions of the lactate dehydrogenase assay kit. The absorbance value was measured at a wavelength of 450 nm using a microplate reader. LDH activity in the sample was determined according to the following equation.

$$\text{LDH activity in the sample (UL}^{-1}\text{)} = \frac{\text{Test sample OD value} - \text{Control OD value}}{\text{Standard OD value} - \text{Blank OD value}} \times \text{Sample standard concentration (0.2 } \mu\text{mol mL}^{-1}\text{)} \times 1000$$

2.9 Statistical analysis

All experimental data were statistically analyzed and drawn using Origin 2021 and Image J software and presented as the means \pm SD. Date differences were analyzed using one-way analysis of variance (ANOVA) and Tukey's analysis. $P < 0.05$ was considered statistically significant.

3. Results and discussion

By adjusting the electrospinning parameters, such as collection distance, applied voltage, solution concentration, and flow rate, we could successfully prepare BNDSs with different molecular weights (HAMA-150k and HAMA-400k) *via* blend and coaxial electrospinning techniques. The obtained scaffold was a white uniform film with a thickness of approximately 100–200 μm , which was the same as the thickness of the natural dura mater. In addition, the microstructures of different scaffolds were further observed using SEM. Fig. 1a–c show the surface morphology of the BNDSs. All electrospun nanofibers were randomly arranged in the interwoven fiber networks, forming smooth surfaces containing micrometer-sized pores, which were reported to play an essential role in tissue ingrowth. The fiber diameters of all BNDSs were mainly in the range of 500–700 nm. In addition, the surfaces of all scaffolds were tightly packed with no obvious clusters or aggregates. Fig. 1d shows the coaxial nanofibers obtained with PCL and RB (red) in the shell and HAMA-150k and FITC-BSA (green) in the core. The fluorescence merge images showed that the core-shell structure had been successfully prepared. Therefore, the core-shell structure of BNDSs was successfully designed using the above method.

As a dural substitute, BNDS requires excellent mechanical properties to maintain intracranial pressure, prevent cerebrospinal fluid leakage, and protect the brain from external mechanical shocks and stresses.^{45,46} Zwirner *et al.* investigated that the tensile strength was 7 MPa \pm 4 MPa and the maximum strain was 11% \pm 3%.⁴⁷ McGarvey *et al.* provided that the mean tensile strength of human cranial dura mater was 9.41 \pm

1.54 MPa and the Young's modulus was 61.50 \pm 9.60 MPa.⁴⁸ More recently, Kizmazoglu *et al.* have found the mean tensile strength of 6.37 \pm 1.94 MPa and the mean Young's modulus of 54.16 \pm 4.82 MPa.⁴⁹ To explore the mechanical properties of BNDSs, we investigated the effects of different molecular weights (HAMA-150k and HAMA-400k) and electrospinning techniques (blend and coaxial) on the mechanical properties of BNDSs. The tensile strengths (Fig. 2a and b) of PCL/HAMA-150k-B/IGF, PCL/HAMA-400k-B/IGF, and PCL/HAMA-150k-C/IGF were 99.53 \pm 6.70 MPa, 107.50 \pm 10.09 MPa, and 105.41 \pm 19.91 MPa, respectively, which indicated that the strength of the scaffolds was good and could resist relatively high stresses. In addition, the elongations (Fig. 2c) at the break of the three groups were 56.96 \pm 4.62%, 67.24 \pm 2.65%, and 63.91 \pm 10.13%, respectively. Both elongations at the break of the scaffolds remained at nearly 60% without significant difference, showing high toughness. They were easy to bend, patch, and cut under practical operating conditions. The Young's modulus (Fig. 2d) of the three groups was 38.60 \pm 0.13 MPa, 34.54 \pm 0.80 MPa, and 23.40 \pm 0.46 MPa, respectively. The

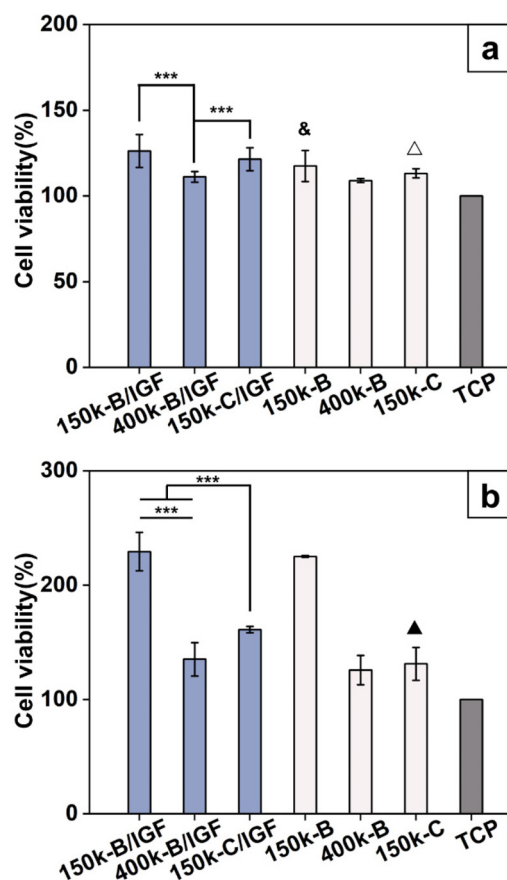


Fig. 5 Cell viability after neurite transection. Cell viability was quantitatively measured using cell counting kit-8 (CCK-8). The cell viability of each group after (a) 1 day and (b) 3 days. There were significant differences between TCP and other groups. *** $P < 0.001$; & $P < 0.05$, $\Delta P < 0.01$, and $\blacktriangle P < 0.001$ when compared with the +IGF group. Notes: TCP served as the control group.

mechanical strength of the scaffolds prepared using the blend electrospinning method was significantly higher than that of the scaffolds prepared using the coaxial electrospinning method, which provided more powerful support for the brain. Besides, a reduction of the HAMA molecular weight could also strengthen the scaffolds.

The contact angles of the three BNDS groups are shown in Fig. S1a.† Generally, a contact angle $>90^\circ$ indicates that the

material is hydrophobic, while a larger contact angle means a more hydrophobic material.⁴⁵ In this study, the water contact angles of PCL/HAMA-150k-B/IGF, PCL/HAMA-400k-B/IGF, and PCL/HAMA-150k-C/IGF were $103.44 \pm 10.23^\circ$, $112.40 \pm 4.91^\circ$, and $119.17 \pm 6.83^\circ$, respectively, thus indicating that BNDSs have good hydrophobicity and can resist water infiltration, which was beneficial for preventing cerebrospinal fluid leakage. Besides, the fiber diameter distribution of the BNDSs

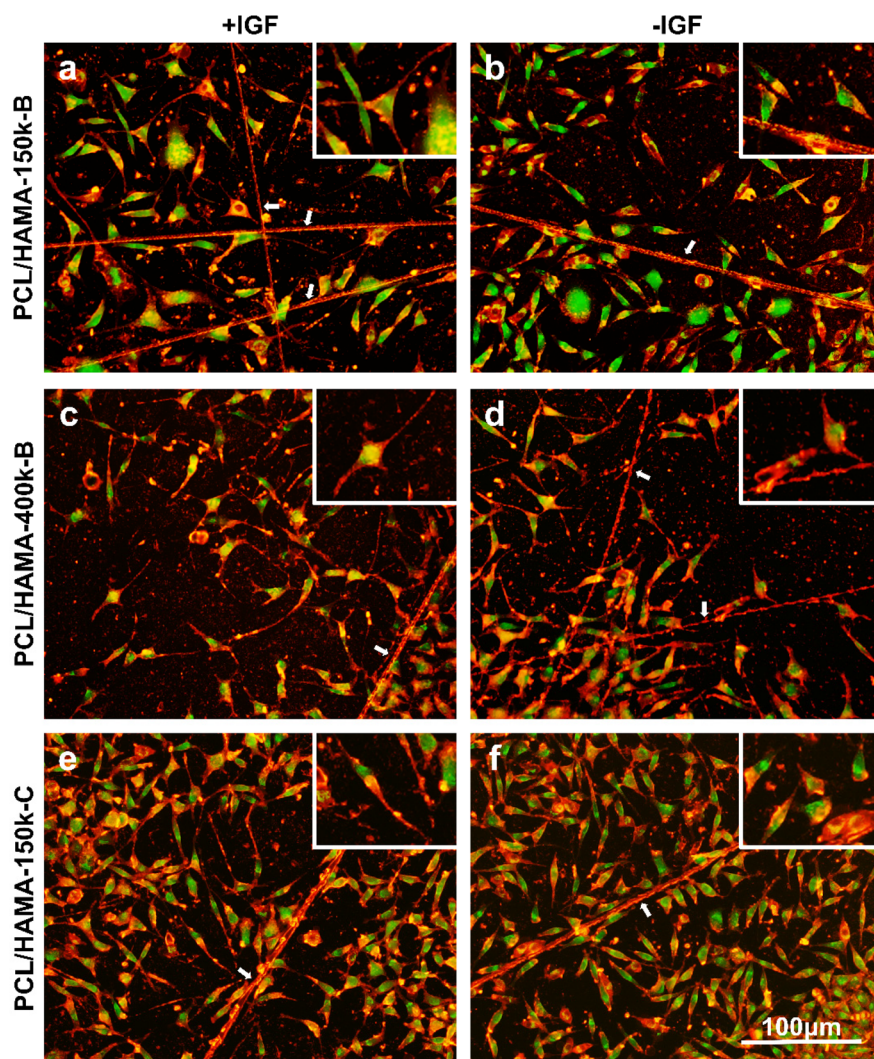


Fig. 6 Neurite outgrowth staining after neurite transection. Fluorescence staining micrographs showing the SH-SY5Y cells after neurite transection and are treated with different BNDSs for 3 days. The cell viability was indicated in green, and the cell membrane was stained in red. The neurite transection was indicated by the white arrows. Enlarged images are shown in the upper right corner. (a) PCL/HAMA-150k-B/IGF; (b) PCL/HAMA-150k-B; (c) PCL/HAMA-400k-B/IGF; (d) PCL/HAMA-400k-B; (e) PCL/HAMA-150k-C/IGF; and (f) PCL/HAMA-150k-C.

Table 1 Neurite length and number of SH-SY5Y cells after neurite transection treatment

	PCL/HAMA-150k-B/IGF	PCL/HAMA-400k-B/IGF	PCL/HAMA-150k-C/IGF	PCL/HAMA-150k-B	PCL/HAMA-400k-B	PCL/HAMA-150k-C	TCP
Average neurite length (μm)	66.3 ± 27.6	63.8 ± 54.5	59.5 ± 26.9	42.9 ± 22.1	45.5 ± 19.3	43.8 ± 22.2	34.0 ± 14.6
Neurite number	2.5 ± 0.8	2.5 ± 0.8	2.4 ± 0.7	1.4 ± 0.7	1.8 ± 0.8	1.9 ± 0.6	1.7 ± 0.6

Related to Fig. 6.

is shown in Fig. S1b–d.† Among them, the average fiber diameters of PCL/HAMA-150k-B/IGF, PCL/HAMA-400k-B/IGF, and PCL/HAMA-150k-C/IGF were $0.37 \pm 0.09 \mu\text{m}$, $0.43 \pm 0.07 \mu\text{m}$, and $0.66 \pm 0.13 \mu\text{m}$, respectively. The average diameter of the coaxial nanofibers was slightly increased compared to the average diameter of the blend nanofibers.

We plotted the cumulative release percentage curves to study the *in vitro* release behavior of the BNDSS (Fig. 3). The curves showed a biphasic pattern with an initial burst release (rapid-release) on the first day, followed by a sustained release (slow-release) over 45 days. On day 1, the cumulative release percentages of PCL/HAMA-150k-B/IGF, PCL/HAMA-400k-B/IGF, and PCL/HAMA-150k-C/IGF were 62%, 52%, and 42%, respectively. After 7 days, more than 65% of RB was released from the scaffolds. The release was faster in the blend group than in the coaxial group. There was still a sustained and increasingly slow release from days 7 to 45, with approximately 100% release from all the three groups on day 45. The rapid release of IGF-1 on day 1 reduces irreversible brain damage from primary damage. The sustained slow-release of IGF-1 for up to 45 days can reduce secondary damage through the neuroprotection of IGF-1. Therefore, the bioactive artificial dural substitute can improve the prognosis of TBI by reducing primary and secondary damage caused by brain injury in the postoperative period through rapid-release and a long-term release of IGF-1.

We investigated the *in vitro* degradation profiles of the BNDSS by simulating a neutral *in vivo* environment. As shown in Fig. 4a, the pH value of PBS in the three groups did not change over 360 days, implying that the BNDSS do not affect the pH of the environment. Additionally, 360-day weight loss curves of BNDSS are shown in Fig. 4b. All the scaffolds showed a slight weight loss after 360 days, including PCL/HAMA-150k-C/IGF by 1 mg, and PCL/HAMA-150k-B/IGF and PCL/HAMA-400k-B/IGF by 4 mg. To further understand the degradation process of the artificial dural scaffolds, we measured the degradational mechanical properties, including tensile strength, elongation at break, and Young's modulus of all the scaffolds at 180 days and 360 days (Table S1†). The results showed that the mechanical performance of these scaffolds was degraded but was sufficient for the targeted application of a previous study.^{47–49} On top of that, we observed the surface morphology of BNDSS after 30 days (Fig. 4c–e) and 180 days (Fig. 4f–h) of degradation using SEM (more SEM images at other times are shown in Fig. S2†). All scaffolds maintained stable microstructures, and the surface morphology remained unchanged for 180 days. The results showed that the degradational mechanical properties of the BNDSS decreased. However, SEM images showed that the BNDSS maintain stable microstructures, which could provide sufficient long-term support during the degradation process. The BNDSS provided support for more than one year, promoting the restoration of normal dural anatomy, remodeling the cranial cavity confinement, preventing CSF leaks, and protecting the brain tissue. It was significantly beneficial for the growth of the dura mater and extraordinarily critical for dural repair. However, longer

degradation cycles are needed to further study the degradation process and explore their degradation kinetics.

Neurite transection was used to simulate primary injury, and SH-SY5Y cells were used to establish a neurite transection model. Cell proliferation was detected before and 24 hours after neurite transection. The result is shown in Fig. S3,† there was no significant difference between the control group and the neurite transection group, indicating that neurite transection only severed the neurite and had no effect on cell viability. In addition, as shown in Fig. S4,† the neurites of the cells before and 24 hours after neurite transection were stained. Fig. S5† shows that the neurite length was significantly reduced, but there was no significant difference in the neurite number at 24 hours post-neurite transection. The above results suggested that neurite transection could reduce the length of neurites but has little effect on the neurite number and cell viability.

To assess the effect of BNDSS on cell viability after neurite transection, we measured the cell viability of each group after neurite transection (Fig. 5). On the first day, the cell viability of

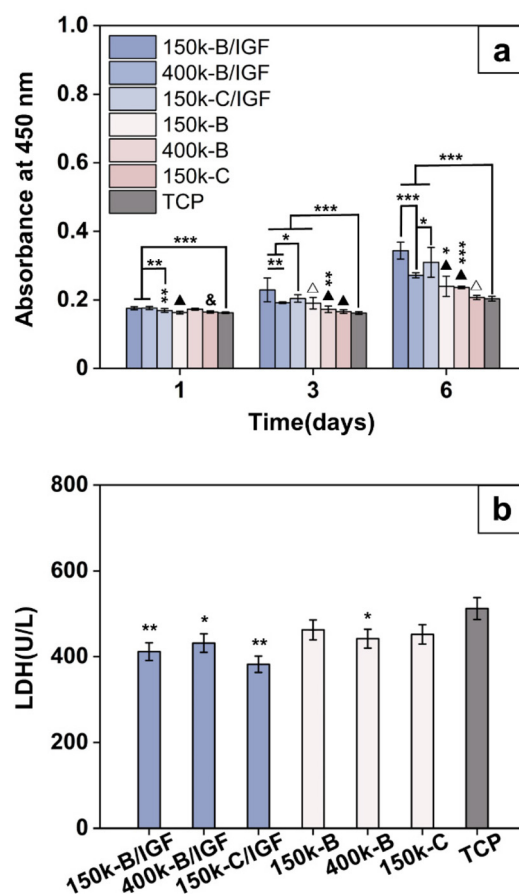


Fig. 7 Oxygen and glucose deprivation (OGD) experiment. (a) Cell viability of SH-SY5Y cells after OGD treatment. (b) Lactate dehydrogenase (LDH) content of SH-SY5Y cells after OGD treatment. * $P < 0.05$, ** $P < 0.01$, and *** $P < 0.001$ compared with the TCP group. & $P < 0.05$, $\Delta P < 0.01$, and $\blacktriangle P < 0.001$ compared with the +IGF group. Notes: TCP served as the control group.

+IGF groups (PCL/HAMA-150k-B/IGF, PCL/HAMA-400k-B/IGF, and PCL/HAMA-150k-C/IGF) and -IGF groups (PCL/HAMA-150k-B, PCL/HAMA-400k-B, and PCL/HAMA-150k-C) were significantly higher than that of the control group. The cell activity in the +IGF groups was higher than in the -IGF groups due to the contribution of IGF-1 to neuroprotection. Furthermore, the cell viability of the PCL/HAMA-150k-B/IGF

group was higher than those of the PCL/HAMA-400k-B/IGF and PCL/HAMA-150k-C/IGF group, indicating a faster release of IGF-1 in the blend group and a better effect of low molecular weight HAMA. The results on day 3 and day 1 showed the same trend, but the figure showed that the number of cells increased with the culture time. In addition, the cell viability on day 3 was significantly higher than on day 1. It was proved

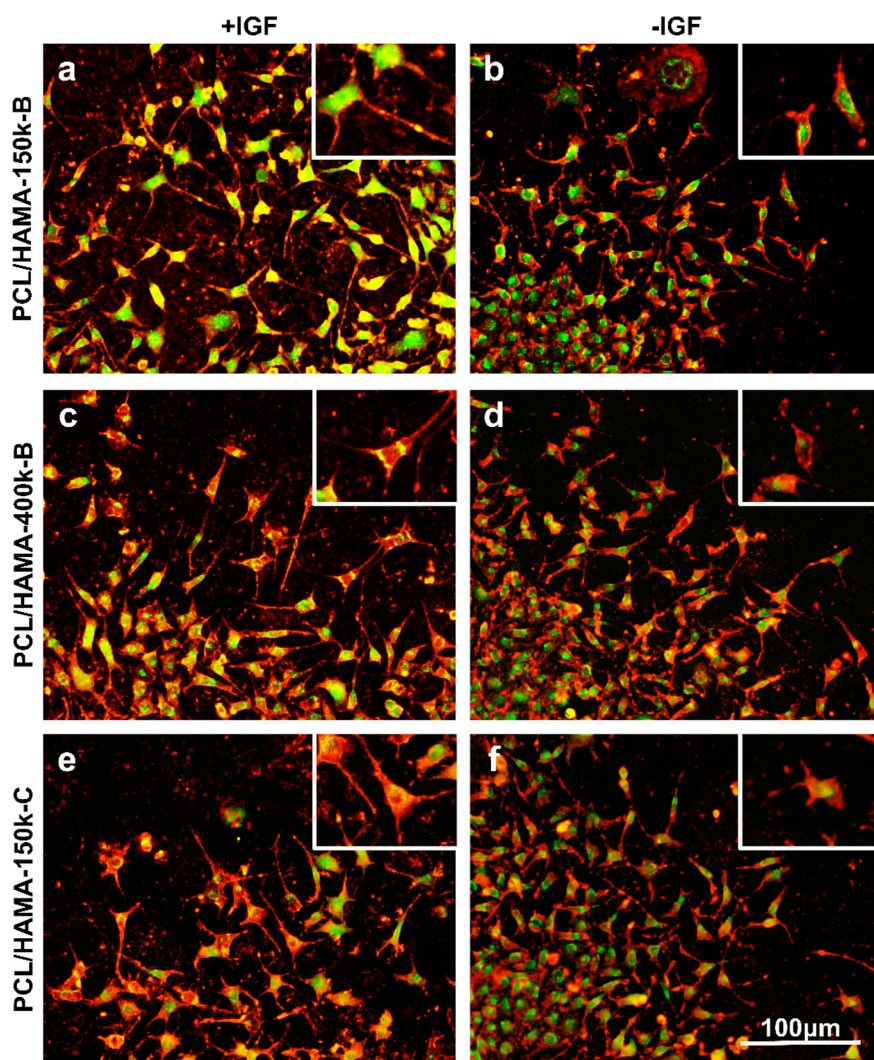


Fig. 8 Neurite outgrowth staining after OGD treatment. The fluorescence staining micrographs showing the SH-SY5Y cells after OGD and treated with different BNDs for 3 days. The cell viability was indicated in green, and the cell membrane was stained in red. Enlarged images are shown in the upper right corner. (a) PCL/HAMA-150k-B/IGF; (b) PCL/HAMA-150k-B; (c) PCL/HAMA-400k-B/IGF; (d) PCL/HAMA-400k-B; (e) PCL/HAMA-150k-C/IGF; and (f) PCL/HAMA-150k-C.

Table 2 Neurite length and number of SH-SY5Y cells after OGD treatment

	PCL/HAMA-150k-B/IGF	PCL/HAMA-400k-B/IGF	PCL/HAMA-150k-C/IGF	PCL/HAMA-150k-B	PCL/HAMA-400k-B	PCL/HAMA-150k-C	TCP
Average neurite length (μm)	64.1 ± 32.0	60.8 ± 31.2	59.2 ± 32.1	57.1 ± 21.9	61.6 ± 29.1	58.0 ± 17.9	41.1 ± 17.9
Neurite number	2.5 ± 0.8	2.8 ± 1.1	2.5 ± 0.9	1.7 ± 0.6	1.4 ± 0.6	1.4 ± 0.5	1.7 ± 0.8

Related to Fig. 8.

that the BNDSSs had excellent biocompatibility and promoted the proliferation of cells after neurite transection.

Fig. 6 and Fig. S6a† show the cell fluorescence staining diagram of cells after transection and treatment with different BNDSSs for 3 days, and the results of statistical analysis are shown in Table 1. The results showed that the average neurite lengths of the +IGF groups and –IGF groups were higher than that of the control group. Since IGF-1 promotes neurite elongation, the neurite length in the +IGF group was longer than in the –IGF group. Furthermore, the neurite length in the PCL/HAMA-150k-B/IGF group was longer than those in the PCL/HAMA-400k-B/IGF and PCL/HAMA-150k-C/IGF groups. The average number of neurites in the +IGF groups was more significant than in the control group. In contrast, the number of neurites in the –IGF groups and control group did not change significantly, suggesting that IGF-1 could increase the number of neurites. Therefore, the BNDSSs had good biocompatibility and could promote cell proliferation and neurite growth after neurite transection, and the +IGF groups were better than the –IGF groups, especially the PCL/HAMA-150K-B/IGF group.

In addition to the primary injury, TBI can also cause secondary injury within minutes to days after the brain injury.⁵⁰ The secondary injury often results in neuronal damage, which leads to impairment of physical function, such as cognitive, motor, and language function.^{2,51,52} TBI produces an inflammatory response in the cells under ischemic and hypoxic conditions. Therefore, we used SH-SY5Y cells to establish an OGD cell model by simulating the secondary injury through the OGD experiment. To evaluate the effect of BNDSSs on cell viability after OGD treatment, we measured the cell viability of each group after OGD treatment. The results showed that the cell viability of the +IGF groups was significantly higher than that of the control group on days 1, 3, and 6, indicating that the BNDSSs prepared with bioactive factor IGF-1 could promote the proliferation of OGD-treated cells, especially in the PCL/HAMA-150K-B/IGF group (Fig. 7a). In addition, it is recognized that LDH is an important enzyme in the body's energy metabolism, which exists widely in various tissues and organs. There was a positive correlation between the level of LDH in CSF and the degree of injury. Therefore, the LDH content in the medium on day 6 after OGD was also measured.^{53,54} The results revealed that the LDH content in the culture medium of the +IGF groups was significantly lower than that of the control group, indicating that the BNDSSs had a positive regulatory effect on the microenvironment after the secondary injury (Fig. 7b).

Fig. 8 and Fig. S6b† show the fluorescence staining diagram of the cells after OGD and treated with different BNDSSs for 3 days. The statistical analysis results in Table 2 show that the average neurite lengths of the +IGF groups and –IGF groups were higher than that of the control group. The average neurite length in the +IGF groups was higher than in the –IGF groups. This was because IGF-1 could promote the elongation of neurites. The average neurite length in the PCL/HAMA-150k-B/IGF group was higher than those in the PCL/HAMA-400k-B/IGF and PCL/HAMA-150k-C/IGF groups. The

average number of neurites in the +IGF groups was more significant than in the control group, while the difference between the –IGF and control groups was insignificant. It was suggested that IGF-1 coated with the BNDSS could increase the number of neurites.

In addition to SH-SY5Y cells, we cultured primary rat cortical neurons (Fig. S7†) to better mimic the cellular environment in the brain. We selected the PCL/HAMA-150K-B/IGF group and the PCL/HAMA-150K-B group as the experimental groups and validated the neuroprotective effect of the BNDSSs with primary cortical neurons through neurite transection and OGD experiment. The cell viability of the primary neurons co-cultured with the BNDSSs after neurite transection and OGD treatment is shown in Fig. 9. The results showed that the cell viability of the PCL/HAMA-150K-B/IGF group and PCL/HAMA-150K-B group was higher than the control group. In particular, on day 6, the cell viability of the control group decreased significantly, while that of the PCL/HAMA-150K-B group decreased slightly. However, the PCL/HAMA-150K-B/IGF group

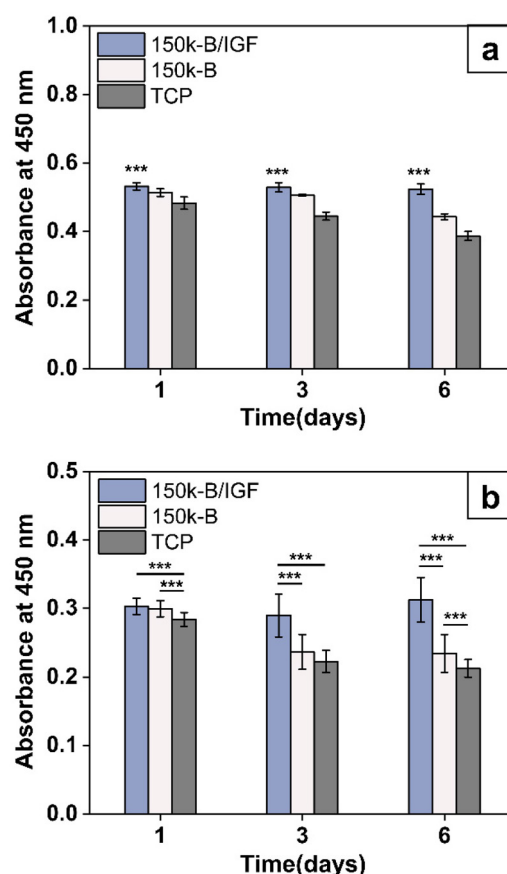


Fig. 9 Cell viability of the primary neurons co-cultured with the BNDSSs after neurite transection and OGD treatments, respectively. (a) Cell viability of primary neurons after neurite transection. *** indicates the significant difference at $P < 0.001$ compared with the other groups. (b) Cell viability of primary neurons after OGD treatment. *** indicates the significant difference at $P < 0.001$ between the different groups. Notes: TCP served as the control group.

HAMA-150K-B/IGF group showed a little decrease after neurite transection and OGD treatment. Generally, it is well known that MAP-2 and synaptophysin are specific markers for neurons and synapses. To demonstrate the neurons formed functional neurite outgrowth, we co-labeled neurons with the presynaptic marker synaptophysin and the neuronal marker MAP-2.^{55–57} Fig. 10 and 11 show the neurite outgrowth staining diagrams and functional investigation. The neurons were treated with different BNDs for 3 days after neurite transection and OGD, respectively. The statistical analysis results are shown in Tables 3 and 4. The results demonstrate that the average neurite length of the experi-

mental groups has an obvious growth compared with the control group, especially the PCL/HAMA-150K-B/IGF group. However, there was little change in the average neurite number. This was consistent with the SH-SY5Y cells above, indicating that the BNDs could promote cell proliferation and neurite growth and improve the microenvironment after the primary and secondary injuries. In conclusion, the prepared BNDs could promote cell proliferation and neurite growth after neurite transection and OGD treatment, and the +IGF groups carrying bioactive factor IGF-1 were superior to the –IGF groups, especially the PCL/HAMA-150K-B/IGF group.

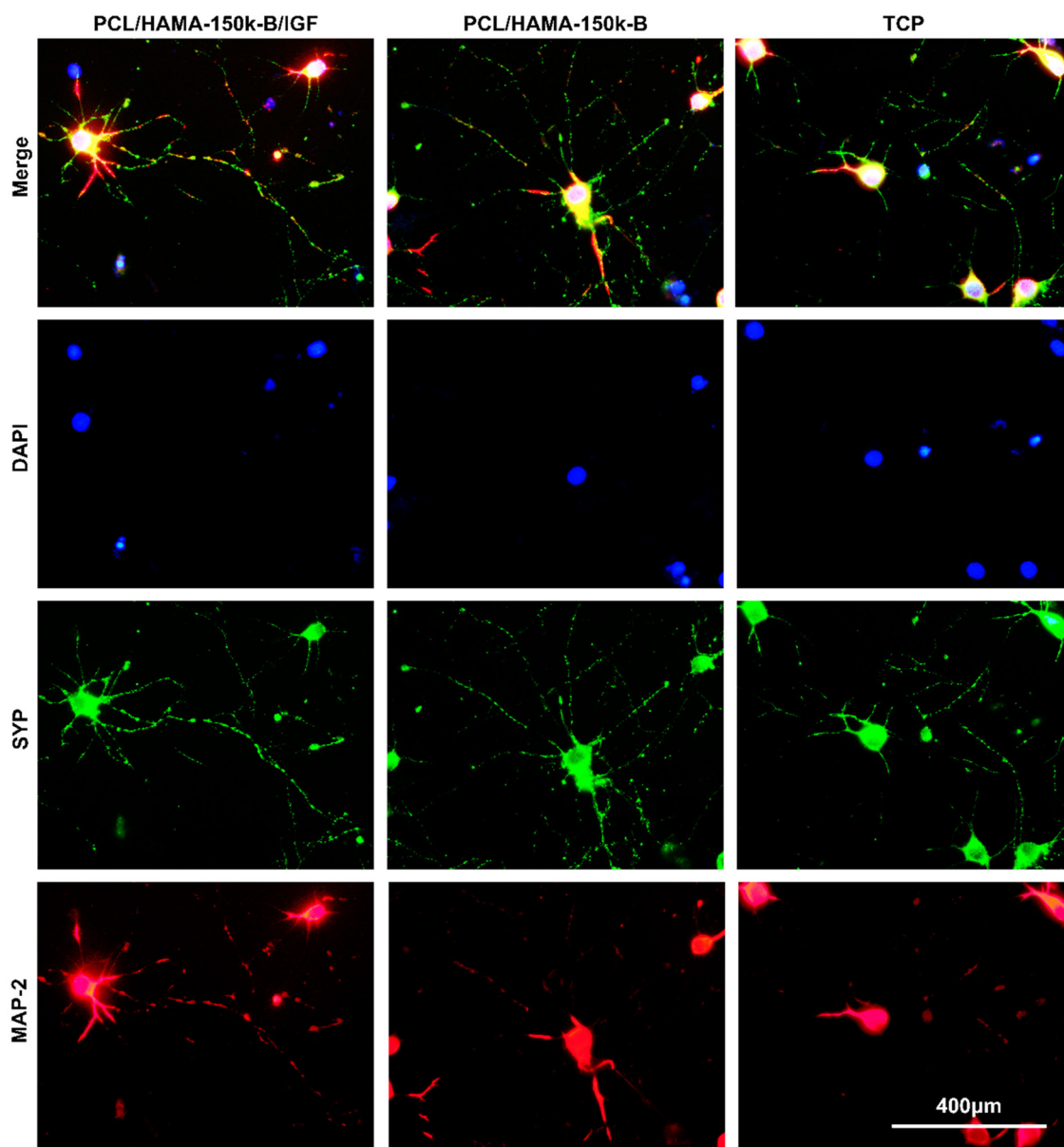


Fig. 10 Neurite outgrowth staining and functional investigation after neurite transection and treated with different BNDs. Immunofluorescence images of the primary neurons after neurite transection and treated with different BNDs for 3 days: DAPI (blue), SYP (green), MAP-2 (red), and merged illustration.

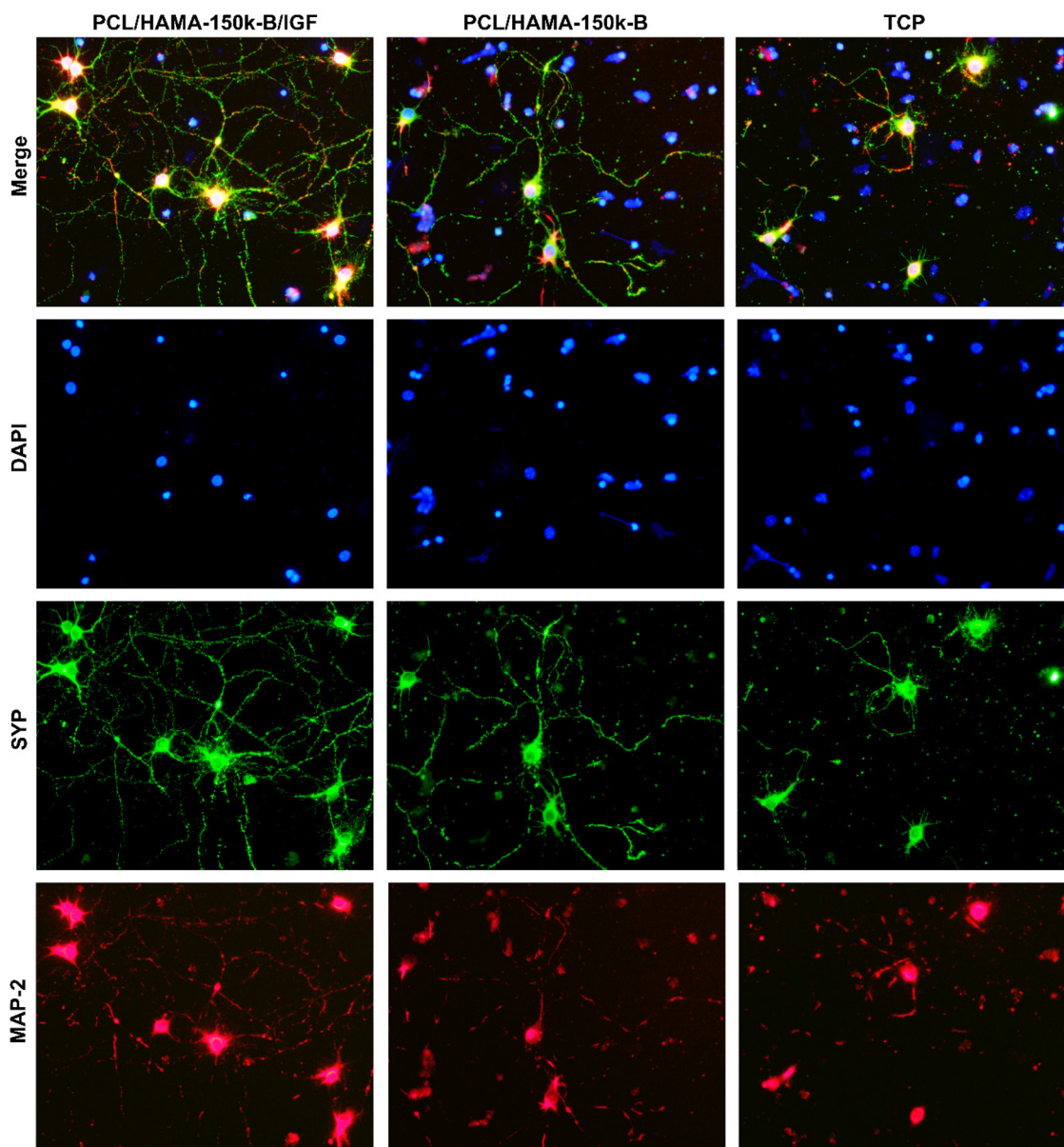


Fig. 11 Neurite outgrowth staining and functional investigation after OGD and treated with different BNDSS. The immunofluorescence images of the primary neurons after OGD and treated with different BNDSSs for 3 days: DAPI (blue), SYP (green), MAP-2 (red), and merged illustration.

Table 3 Neurite length and number of primary neurons after neurite transection treatment

	PCL/HAMA-150k-B/IGF	PCL/HAMA-150k-B	TCP
Average neurite length (μm)	114.34 ± 61.90	54.59 ± 41.50	27.30 ± 15.30
Neurite number	4.23 ± 1.69	3.77 ± 1.35	3.56 ± 1.25

Related to Fig. 10.

Table 4 Neurite length and number of primary neurons after OGD treatment

	PCL/HAMA-150k-B/IGF	PCL/HAMA-150k-B	TCP
Average neurite length (μm)	102.15 ± 66.06	46.55 ± 46.51	17.77 ± 9.92
Neurite number	5.24 ± 1.82	5.07 ± 1.81	3.82 ± 1.52

Related to Fig. 11.

4. Conclusion

In this study, a series of bioactive nanofibrous dural substitutes were designed and manufactured using coaxial or blend

electrospinning techniques to investigate their potential use in neuroprotection after decompressive craniectomy of TBI. The biocompatibility, surface morphology, mechanical properties, and hydrophobicity were characterized, and the results showed

that such nanofibrous scaffolds were suitable for dural substitutes. *In vitro* release and degradation behaviors showed that the bioactive artificial dura mater could provide sufficient long-term structural support during the degradation process and maintain a long-time sustained release of IGF-1. Further investigations demonstrated that they could also promote neural cell survival, improve the microenvironment of neurite growth, and play an important role in the neuroprotective effect after the primary and secondary injuries, particularly the PCL/HAMA-150k-B/IGF group. In summary, such bioactive nanofibrous dural substitutes exhibited great potential in practical application for neuroprotection in the case of dural repair, providing promising alternatives to neurosurgery involving artificial dura mater.

Conflicts of interest

The authors declare no competing financial interests.

Acknowledgements

This work was supported by the National Natural Science Foundation of China (32171322, 82001970), the Natural Science Foundation of Shandong Province (ZR2021YQ17), the Young Elite Scientists Sponsorship Program by CAST (No. YESS20200097), the Science and Technology Guiding Project of China National Textile and Apparel Council (2021054), the Qingdao Health Science and Technology Plan Project (2020-WJZD143), the Qingdao Key Health Discipline Development Fund (2020–2022), and the Qingdao Clinical Research Center for Oral Diseases (22-3-7-lczx-7-nsh).

References

- M. K. Shin, E. Vázquez-Rosa, Y. Koh, M. Dhar, K. Chaubey, C. J. Cintrón-Pérez, S. Barker, E. Miller, K. Franke, M. F. Noterman, D. Seth, R. S. Allen, C. T. Motz, S. R. Rao, L. A. Skelton, M. T. Pardue, S. J. Fliesler, C. Wang, T. E. Tracy, L. Gan, D. J. Liebl, J. P. J. Savarraj, G. L. Torres, H. Ahnstedt, L. D. McCullough, R. S. Kitagawa, H. A. Choi, P. Zhang, Y. Hou, C. W. Chiang, L. Li, F. Ortiz, J. A. Kilgore, N. S. Williams, V. C. Whitehair, T. Gefen, M. E. Flanagan, J. S. Stamler, M. K. Jain, A. Kraus, F. Cheng, J. D. Reynolds and A. A. Pieper, *Cell*, 2021, **184**, 2715–2732.
- J. Ginsburg and J. S. Huff, *StatPearls*, StatPearls Publishing Copyright © 2022, StatPearls Publishing LLC, Treasure Island (FL), 2022.
- Y. Jing, X. Ma, C. Xu, H. L. Tian and S. W. Chen, *Mater. Sci. Eng., C*, 2020, **117**, 111246.
- X. Bi, B. Liu, Z. Mao, C. Wang, N. Dunne, Y. Fan and X. Li, *Mater. Sci. Eng., C*, 2020, **117**, 111326.
- S. K. He, J. H. Guo, Z. L. Wang, Y. Zhang, Y. H. Tu, S. Z. Wu, F. G. Huang and H. Q. Xie, *Mater. Sci. Eng., C*, 2017, **73**, 267–274.
- G. Cao, Y. Huang, K. Li, Y. Fan, H. Xie and X. Li, *J. Mater. Chem. B*, 2019, **7**, 5038–5055.
- Q. Li, L. Mu, F. Zhang, Y. Sun, Q. Chen, C. Xie and H. Wang, *Mater. Sci. Eng., C*, 2017, **80**, 346–351.
- Z. N. Litvack, G. A. West, J. B. Delashaw, K. J. Burchiel and V. C. Anderson, *Neurosurgery*, 2009, **65**, 890–897; discussion 897.
- K. E. Flanagan, L. W. Tien, R. Elia, J. Wu and D. Kaplan, *J. Biomed. Mater. Res., Part B*, 2015, **103**, 485–494.
- M. Oria, R. R. Tatu, C. Y. Lin and J. L. Peiro, *J. Surg. Res.*, 2019, **242**, 62–69.
- Z. Shi, T. Xu, Y. Yuan, K. Deng, M. Liu, Y. Ke, C. Luo, T. Yuan and A. Ayyad, *Artif. Organs*, 2016, **40**, 403–413.
- H. Jiang, Y. Qian, C. Fan and Y. Ouyang, *Front. Bioeng. Biotechnol.*, 2020, **8**, 582646.
- F. Asghari, D. Rabiei Faradonbeh, Z. V. Malekshahi, H. Nekounam, B. Ghaemi, Y. Yousefpoor, H. Ghanbari and R. Faridi-Majidi, *Carbohydr. Polym.*, 2022, **278**, 118926.
- A. Rastegar, M. Mahmoodi, M. Mirjalili and N. Nasirizadeh, *Carbohydr. Polym.*, 2021, **269**, 118351.
- Y. Qian, X. Zhou, F. Zhang, T. G. H. Diekwisch, X. Luan and J. Yang, *ACS Appl. Mater. Interfaces*, 2019, **11**, 37381–37396.
- R. Shi, J. Xue, H. Wang, R. Wang, M. Gong, D. Chen, L. Zhang and W. Tian, *J. Mater. Chem. B*, 2015, **3**, 4063–4073.
- X. Fang, H. Guo, W. Zhang, H. Fang, Q. Li, S. Bai and P. Zhang, *J. Mater. Chem. B*, 2020, **8**, 10593–10601.
- J. C. Silva, R. N. Udangawa, J. Chen, C. D. Mancinelli, F. F. F. Garrudo, P. E. Mikael, J. M. S. Cabral, F. C. Ferreira and R. J. Linhardt, *Mater. Sci. Eng., C*, 2020, **107**, 110291.
- W. Peng, S. Ren, Y. Zhang, R. Fan, Y. Zhou, L. Li, X. Xu and Y. Xu, *Front. Bioeng. Biotechnol.*, 2021, **9**, 668428.
- A. R. Sadeghi-Avalshahr, S. Nokhasteh, A. M. Molavi, N. Mohammad-Pour and M. Sadeghi, *Int. J. Mol. Sci.*, 2020, **21**, 2311.
- J. W. Jung, H. Lee, J. M. Hong, J. H. Park, J. H. Shim, T. H. Choi and D. W. Cho, *Biofabrication*, 2015, **7**, 045003.
- W. M. Tian, C. L. Zhang, S. P. Hou, X. Yu, F. Z. Cui, Q. Y. Xu, S. L. Sheng, H. Cui and H. D. Li, *J. Controlled Release*, 2005, **102**, 13–22.
- P. Wang, S. Huang, Z. Hu, W. Yang, Y. Lan, J. Zhu, A. Hancharou, R. Guo and B. Tang, *Acta Biomater.*, 2019, **100**, 191–201.
- J. A. Burdick and G. D. Prestwich, *Adv. Mater.*, 2011, **23**, H41–H56.
- S. A. Bencherif, A. Srinivasan, F. Horkay, J. O. Hollinger, K. Matyjaszewski and N. R. Washburn, *Biomaterials*, 2008, **29**, 1739–1749.
- Q. Yu, Z. Meng, Y. Liu, Z. Li, X. Sun and Z. Zhao, *Polymers*, 2021, **13**, 2302.
- B. Velasco-Rodriguez, T. Diaz-Vidal, L. C. Rosales-Rivera, C. A. García-González, C. Alvarez-Lorenzo, A. Al-Modlej, V. Domínguez-Arca, G. Prieto, S. Barbosa, J. F. A. Soltero Martínez and P. Taboada, *Int. J. Mol. Sci.*, 2021, **22**, 6758.
- S. Amorim, C. A. Reis, R. L. Reis and R. A. Pires, *Trends Biotechnol.*, 2021, **39**, 90–104.

- 29 T. U. Nguyen, K. E. Watkins and V. Kishore, *J. Biomed. Mater. Res., Part A*, 2019, **107**, 1541–1550.
- 30 M. S. Bae, J. Y. Ohe, J. B. Lee, D. N. Heo, W. Byun, H. Bae, Y. D. Kwon and I. K. Kwon, *Bone*, 2014, **59**, 189–198.
- 31 Y. Zhou, Z. Gu, J. Liu, K. Huang, G. Liu and J. Wu, *Carbohydr. Polym.*, 2020, **230**, 115640.
- 32 D. Chuan, Y. Wang, R. Fan, L. Zhou, H. Chen, J. Xu and G. Guo, *Int. J. Nanomed.*, 2020, **15**, 3729–3740.
- 33 V. E. Bianchi, V. Locatelli and L. Rizzi, *Int. J. Mol. Sci.*, 2017, **18**, 2441.
- 34 R. Wang, H. Bao, S. Zhang, R. Li, L. Chen and Y. Zhu, *Int. J. Biol. Sci.*, 2018, **14**, 1791–1799.
- 35 M. L. Herrera, S. Bandín, L. G. Champarini, C. B. Hereñú and M. J. Bellini, *Brain Res. Bull.*, 2021, **175**, 196–204.
- 36 R. Corne, V. Besson, S. Ait Si Slimane, M. Coutan, M. L. C. Palhas, F. X. Shen, C. Marchand-Leroux, M. Ogier and R. Mongeau, *Neuroscience*, 2021, **466**, 205–221.
- 37 J. Yan, R. Wu, S. Liao, M. Jiang and Y. Qian, *Front. Bioeng. Biotechnol.*, 2020, **8**, 590998.
- 38 X. P. Yang, L. F. Li, D. Z. Yang, J. Nie and G. P. Ma, *Adv. Fiber Mater.*, 2020, **2**, 105–117.
- 39 Y. P. Dong, Y. Q. Zheng, K. Y. Zhang, Y. M. Yao, L. H. Wang, X. R. Li, J. Y. Yu and B. Ding, *Adv. Fiber Mater.*, 2020, **2**, 212–227.
- 40 H. Xu, M. Medina-Sánchez, V. Magdanz, L. Schwarz, F. Hebenstreit and O. G. Schmidt, *ACS Nano*, 2018, **12**, 327–337.
- 41 J. Wang, L. Helder, J. Shao, J. A. Jansen, M. Yang and F. Yang, *Int. J. Pharm.*, 2019, **564**, 1–9.
- 42 D. Cao, R. Xue, J. Xu and Z. Liu, *J. Nutr. Biochem.*, 2005, **16**, 538–546.
- 43 B. Morrison 3rd, B. S. Elkin, J. P. Dollé and M. L. Yarmush, *Annu. Rev. Biomed. Eng.*, 2011, **13**, 91–126.
- 44 K. Hayakawa, E. Esposito, X. Wang, Y. Terasaki, Y. Liu, C. Xing, X. Ji and E. H. Lo, *Nature*, 2016, **535**, 551–555.
- 45 W. Deng, Y. Tan, M. S. Riaz Rajoka, Q. Xue, L. Zhao and Y. Wu, *Carbohydr. Polym.*, 2021, **256**, 117577.
- 46 M. X. Chen, Z. Wang, K. W. Li, X. D. Wang and L. Wei, *Adv. Fiber Mater.*, 2021, **3**, 1–13.
- 47 J. Zwirner, M. Scholze, J. N. Waddell, B. Ondruschka and N. Hammer, *Sci. Rep.*, 2019, **9**, 16655.
- 48 K. A. McGarvey, J. M. Lee and D. R. Boughner, *Biomaterials*, 1984, **5**, 109–117.
- 49 C. Kizmazoglu, H. E. Aydin, I. Kaya, M. Atar, B. Husemoglu, O. Kalemci, G. Sozer and H. Havitioglu, *J. Korean Neurosurg. Soc.*, 2019, **62**, 635–642.
- 50 B. A. Stoica and A. I. Faden, *Neurotherapeutics*, 2010, **7**, 3–12.
- 51 L. Chen, Q. Song, Y. Chen, S. Meng, M. Zheng, J. Huang, Q. Zhang, J. Jiang, J. Feng, H. Chen, G. Jiang and X. Gao, *ACS Nano*, 2020, **14**, 6636–6648.
- 52 D. Sacks, B. Baxter, B. C. V. Campbell, J. S. Carpenter, C. Cognard, D. Dippel, M. Eesa, U. Fischer, K. Hausegger, J. A. Hirsch, M. Shazam Hussain, O. Jansen, M. V. Jayaraman, A. A. Khalessi, B. W. Kluck, S. Lavine, P. M. Meyers, S. Ramee, D. A. Rüfenacht, C. M. Schirmer and D. Vorwerk, *Int. J. Stroke*, 2018, **13**, 612–632.
- 53 D. Si, P. Yang, R. Jiang, H. Zhou, H. Wang and Y. Zhang, *Behav. Brain Res.*, 2014, **264**, 135–142.
- 54 J. Y. Koh and D. W. Choi, *J. Neurosci. Methods*, 1987, **20**, 83–90.
- 55 K. C. Cap, Y. J. Jung, B. Y. Choi, S. J. Hyeon, J. G. Kim, J. K. Min, R. Islam, A. J. Hossain, W. S. Chung, S. W. Suh, H. Ryu and J. B. Park, *Redox Biol.*, 2020, **32**, 101446.
- 56 F. Azizi, H. Jalil, Z. Nasiri, J. Moshtaghian, F. Esmaili, A. Doostmohammadi, L. Shabani and E. Ebrahimie, *J. Tissue Eng. Regener. Med.*, 2018, **12**, 1909–1924.
- 57 K. Takahashi, Q. Kong, Y. Lin, N. Stouffer, D. A. Schulte, L. Lai, Q. Liu, L. C. Chang, S. Dominguez, X. Xing, G. D. Cuny, K. J. Hodgetts, M. A. Glicksman and C. L. Lin, *J. Exp. Med.*, 2015, **212**, 319–332.